JOURNAL OF APPLIED POLYMER SCIENCE VOL. IV, ISSUE NO. 12, PAGES 296-313 (1960)

Instrumentation and Machines for Dynamic Tests

HOWARD A. SCHEETZ,* SEVERINO L. KOH,† and J. NORTON BRENNAN‡

Pennsylvania State University, University Park, Pennsylvania

INTRODUCTION

In the discussion which follows, three main points are considered. The first is that there is no place in a shock and vibration laboratory for a low-pass filter. It has been found that they are not needed, that they can never do any good, and that on the contrary, they may do a great deal of harm by giving us a false sense of confidence in our results. The second point is that a great many of the dynamic testing machines in use, for military specification work for instance, are seriously defective in their design. This opinion is based in part on experience in testing a few different types of machine, in part on visual inspection of other types, in part on the basis of discussions with colleagues, and especially on the basis of the large number of low-pass filters that can be observed in use in laboratories throughout the country. The third point is that this state of affairs is not a necessary one. On the contrary, we can and must redesign our dynamic testing devices to correct the inherent defects that they now have.

Following a brief introduction, the technical portion of this report is presented in two parts. The first part describes the results of using wide-band instrumentation in evaluating an existing testing machine; the second part describes the methods used to overcome some of the more important defects of impact testing devices.

The work to be described was carried out in the Shock and Vibration Laboratory of The Pennsylvania State University as part of a larger program dealing with how things get broken in impact and why. The work was sponsored (under Contracts DA 19-129 QM 386 & 884) by the U. S. Army Quartermaster Corps, Natick R & E Command, which has as one of its missions responsibility for research on air-drop delivery. Their plan, in general terms, was to air-drop equipment and materiel with small parachutes to limit the striking velocity to between 100 and 200 ft./sec. and to use crushable cushioning material to prevent damage from the high-velocity impact at ground contact. The practicality of this plan had already been demonstrated in field tests of a few selected items. In these tests, the amount of cushioning required for each particular item had been determined by trial and error. There existed a need for laboratory method that would determine in advance the amount of cushioning that would be required to protect any specific item under specified impact conditions.

It was recognized at the outset that this was not a simple problem and that a very large amount of basic research would be required before it would be possible to find a really good solution to the practical problem of measuring "fragility" in the laboratory.

Our initial experimental work was divided into four phases: (*1*) dynamic behavior of materials under impulsive loading; (*2*) dynamic response of simple structures under impulsive loading; (*3*) machines for producing impulsive forces; and (*4*) instruments for measuring impulsive forces and motions. In this report, space will permit discussion of only two very small segments of this work, namely, instruments for dynamic materials testing and a drop-tester for light-weight items such as a panel voltmeter.

PART 1. INSTRUMENTATION FOR DYNAMIC TESTING OF MATERIALS AND STRUCTURES*

For our initial work on materials we modified a standard Riehle impact testing machine. In the standard form the user has available one of two energies for the impact (110 ft.-lb. or 220 ft.-lb.).

* Present address: Cornell Aeronautical Laboratory, Buffalo, New York.

† Present address: Purdue University, Lafayette, Indiana.

‡ Present address: Continental Can Company, Chicago, Illinois.

* By Severino L. Koh and J. Norton Brennan.

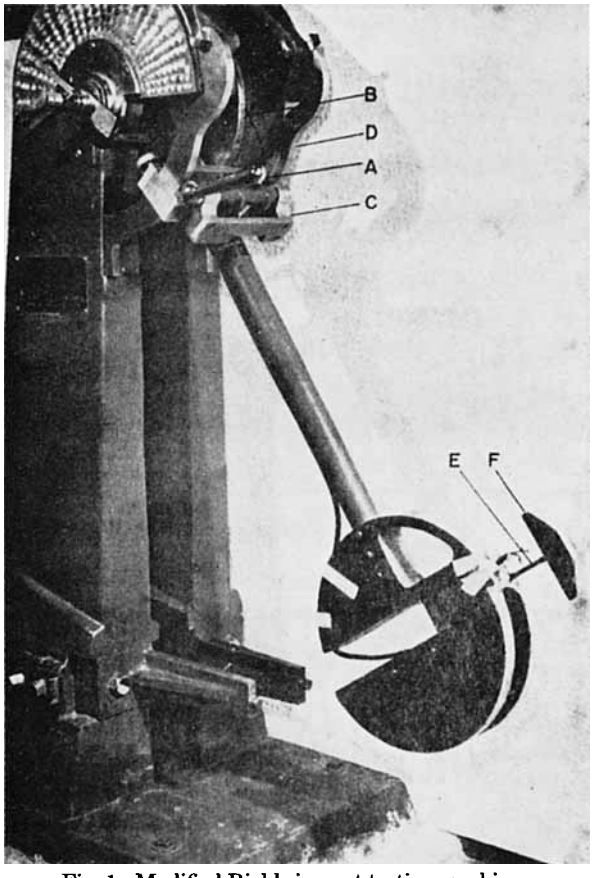

Fig. 1. Modified Riehle impact testing machine.

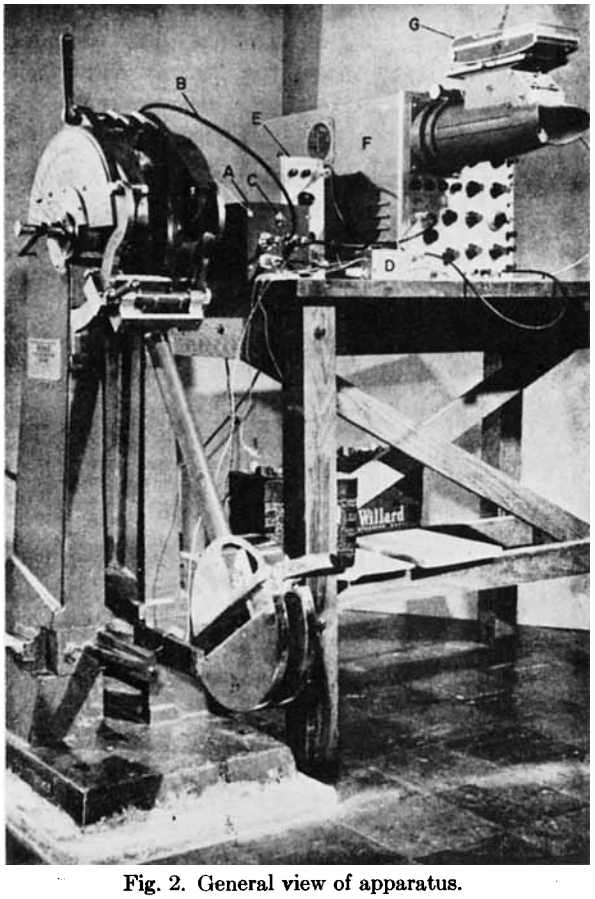

Fig. 2. General view of apparatus.

As we modified the apparatus, the impact energy could be varied continuously from almost zero to 110 ft.-lb. This modification is shown in Figure 1, which shows the variable impact-energy release attachment which was made. The release mechanism, whose handle is shown at (A) has been removed from its normal position at (B) and mounted on a carriage (C) that slides on curved ways (D) and which may be locked at various positions to produce variable amounts of input energy. After impact the pendulum rebounds and is caught by hand and raised again to the ready position. On the specimen (E) are mounted two diametrically opposed strain gages. The crossarm (F) in this view has been rotated from its normal position so that the view of the specimen is not blocked. In an actual test the crossarm would be in a position at right angles to that shown so that it would strike the two anvils shown.

Figure 2 is a general view of the apparatus. The normal position of the crossarm is shown. There is a junction box shown at (A) to which is attached a cable (B) from the strain gages. A switch (C) is provided so that the outputs of the two strain gages may be added together to give a voltage proportional to the axial strain or be opposed so that the voltage produced is proportional to the bending strain. A box (D) contains a resistor used to calibrate the strain gage sensitivity. A Tektronix type 122 preamplifier, shown at (E) is used. Its output is displayed on a Tektronix type 535 oscilloscope (F) and photographed with a Land-Polaroid Camera (G). An accelerometer (not shown) is used to measure the force–time relation.

Figure 3 is a block diagram of the apparatus. In addition to the components already mentioned, it shows the arrangement used to trigger the sweep of the scope in advance of the impact. For the first tests 1018 HR Steel was used. The specimen was the Standard ASTM impact tension specimen.

The first oscillograms obtained were not at all reproducible due to the presence of high-frequency noise. The all too common procedure at this point in the majority of shock and vibration laboratories would be to circumvent the difficulty by utilizing a low-pass filter, i.e., an electrical network that will suppress all frequencies in the signal above the

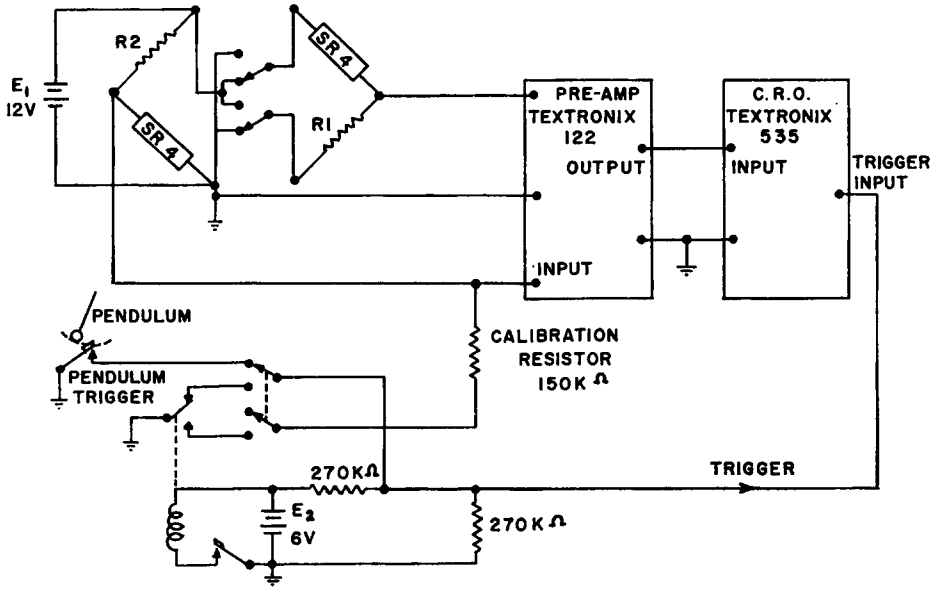

Fig. 3. Schematic diagram of the instrumentation for impact testing of materials.

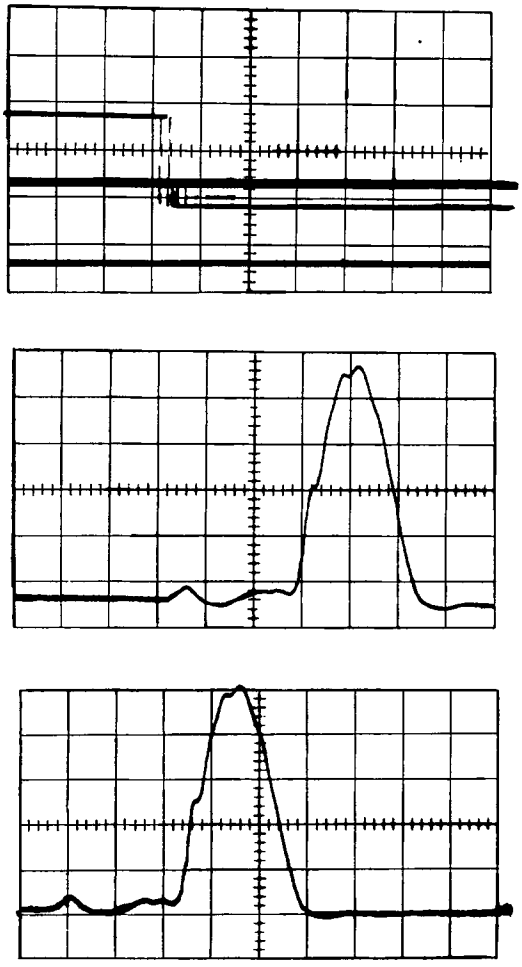

Figure 4.

band pass frequency of the filter. This has been done in the past because it tends to make the signal more reproducible, and the justification for using a filter is that one thereby gets some information rather than none at all. At the same time, it should be recognized that in getting rid of the high-frequency noise we also lose any high-frequency information that may be present as well.

For some engineering applications this may be an acceptable procedure, but for our own problem it was not. Besides, we suspected in advance that the low-pass filter is not really necessary, because, with proper care, the noise can be eliminated at the source.

Such proved to be the case in this instance. We were successful in locating the source of all the electrical noise and eliminating it, and the resulting oscillograms are remarkably clean, considering the wide band pass of the instrumentation used (40 kcycles/sec.).

Figure 4 shows such an oscillogram. These curves show the instantaneous value of the axial strain as a function of time. The step pulse at the top is a calibration pulse with the step equivalent to a strain of 197 μin./in., so that each major division on the vertical scale corresponds to 100 μin./in. Each major division on the horizontal scale corresponds to 1 msec.

Below the curve for the calibration pulse are shown oscillograms for two successive impacts. Theoretically, each should be approximately half of a pure sine wave. After we had eliminated all

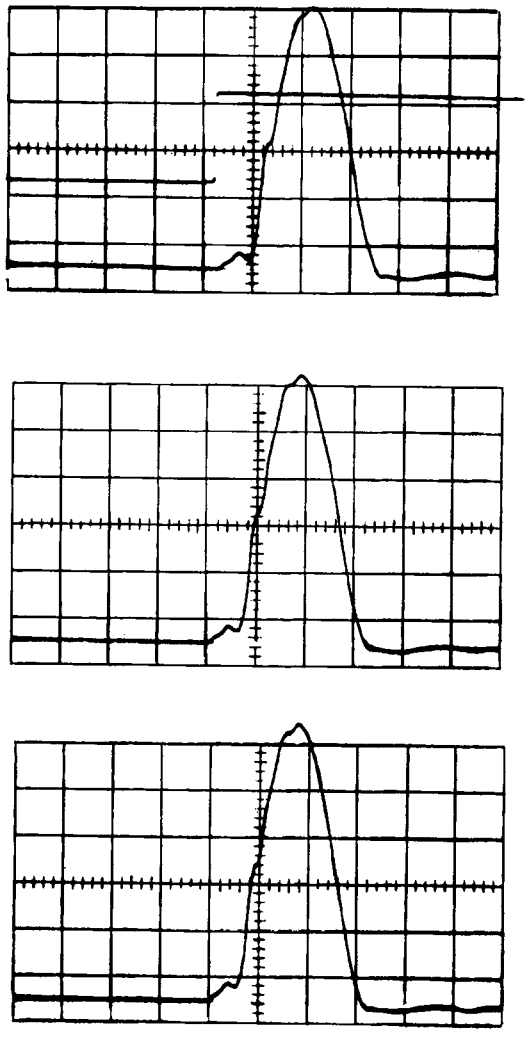

Figure 5.

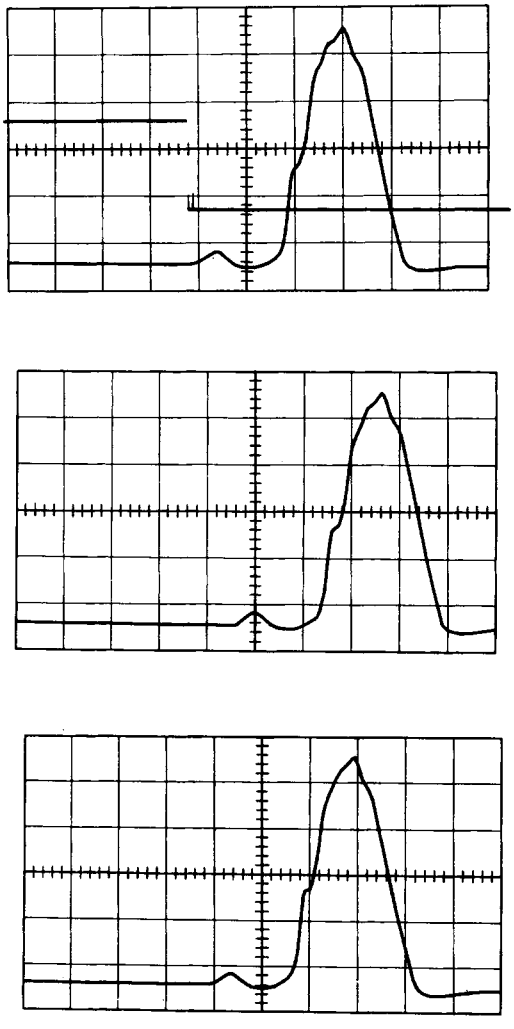

Figure 6.

the sources of electrical noise, the squiggles shown still remained. Note how reproducible the records are. In each case there is a small peak of the same amplitude and at the same time (2.2 msec.) ahead of the start of the main pulse; there is a second disturbance ahead of the main pulse; halfway up the main pulse there is a tiny plateau, and there is a small dip at the peak of the main pulse in each case. Because of the almost perfect reproducibility of the curves it was concluded that the irregularities shown are mechanical in origin rather than electrical. In tracking down the cause it occurred to us that the crossarm might be hitting one anvil ahead of the other. In order to test this idea we inserted a 0.010-in. shim under one of the anvils with the result shown in Figure 5. Here we have three oscillograms, different from those in the previous slide but showing excellent reproducibility among themselves. The most important point is that the small peak preceding the main one is now only 1.2 msec. ahead instead of 2.2 msec. as in the previous slide. We next inserted an additional 0.010-in. shim under the same anvil with the result shown in Figure 6. Now the small peak has begun to merge with the main one. A third shim produced no appreciable change as shown in Figure 7 and a fourth shim inserted under the anvil produced the result shown in Figure 8. Again we have a small peak preceding the main one by 1.0 msec. This has been interpreted to mean that we have over-corrected and are now striking the other anvil first. The obvious next step is to go back to the case when the total thickening of shim was 0.030 in. and to increase the thickness in 0.001 in. increments until optimum performance is achieved. Although this was

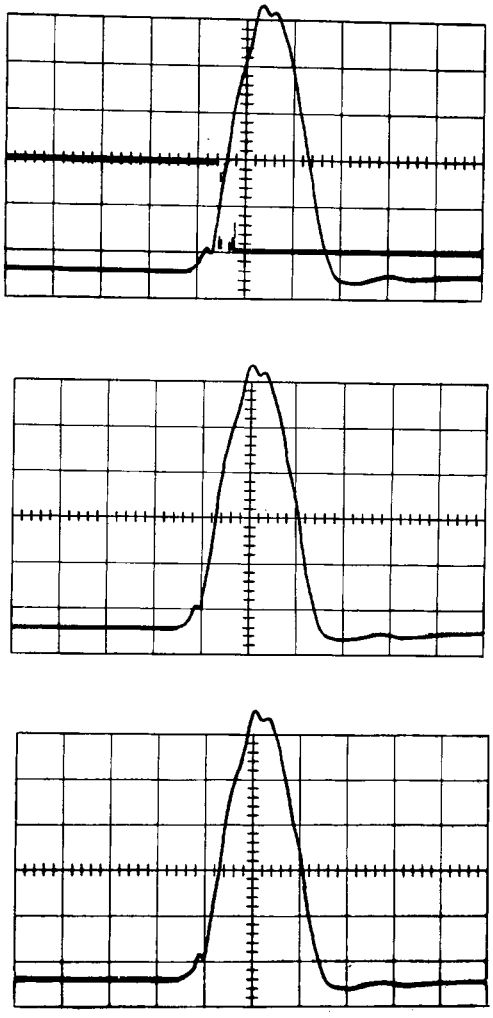

Figure 7.

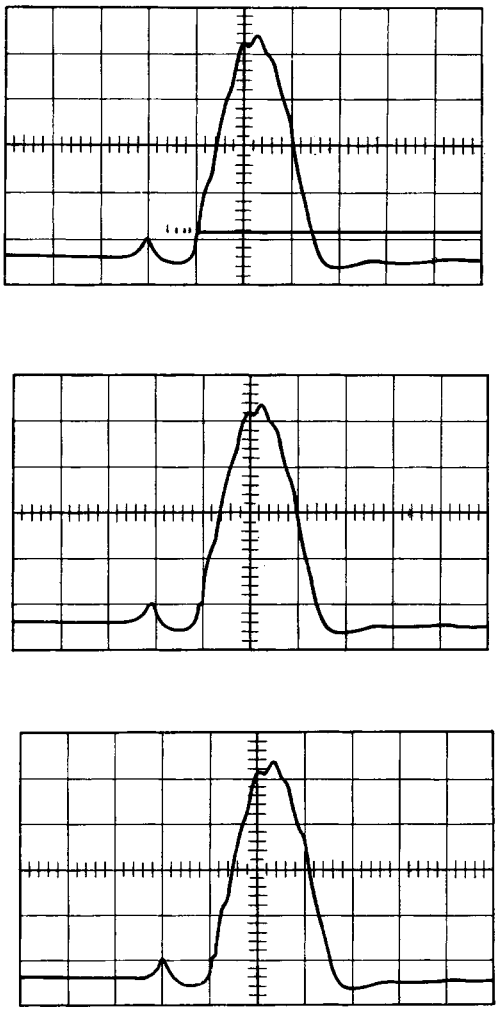

Figure 8.

tried, it was found impossible to eliminate completely the small preliminary peak, principally because of loose-fitting parts in the machine.

In the preceding figures the energy of the impact was maintained constant. In previous tests, where the impact energy was allowed to vary, we had noticed some variation in the duration of the impact, as might be expected.

In order to investigate the duration of the impact we improvised the following arrangement. The crossarm and one of the anvils were made to serve as the two elements of a switch. A voltage drop between the crossarm and anvil is established by passing a small battery-produced current through the body of the machine. This voltage drop is displayed on the dual-channel oscilloscope. When the crossarm touches the anvil, it produces a momentary short circuit that lasts for the duration of the impact, with a corresponding change in the signal observed on the scope. This is shown in Figure 9. The small portion of the record at (A) probably corresponds to the premature contact made on one anvil; the main pulse duration is indicated by the long straight portion of the curve. We did not investigate the cause of the "hash" shown at (B) and (C) since it occurs before and after the main pulse.

Figure 10 shows the oscillograms of three successive impacts of different energy. For the case of the largest energy, the duration is approximately 2.6 msec.; for the medium case it is 3.0 msec.; and for the smallest energy case it is 3.1 msec.

The previous figures have all shown the time variation of the axial strain. On the basis of those oscillograms one might conclude that the testing machine we improvised was a reasonably good de-

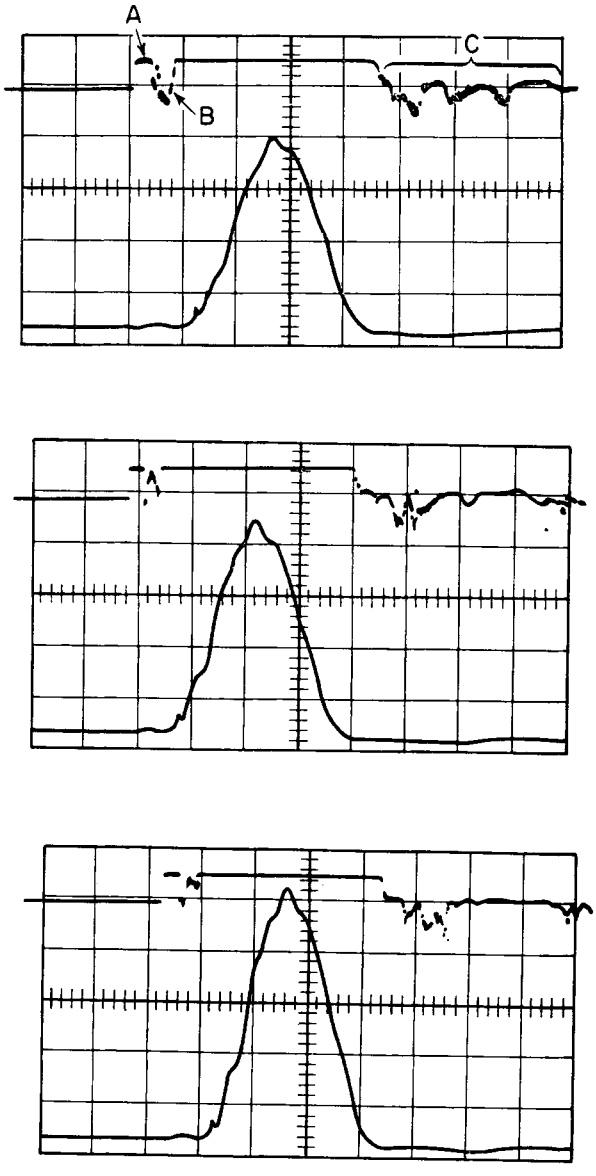

Figure 9.

vice for our work. As soon as the bending strains are examined, however, a different picture comes to light.

In Figure 11 are two sets of oscillograms in which the axial strains are compared to the bending strains. In both sets the uppermost curve shows the axial strain, the middle curve shows the bending strains and the lowest curve is a 60 cycle/sec. timing wave. The tall spike at the left end of the axial strain curve is the main pulse, and the trailing vibrations are small in comparison. The bending vibrations curve is surprisingly large and starts before the main pulse, presumably as a result of the uneven striking of the crossarm.

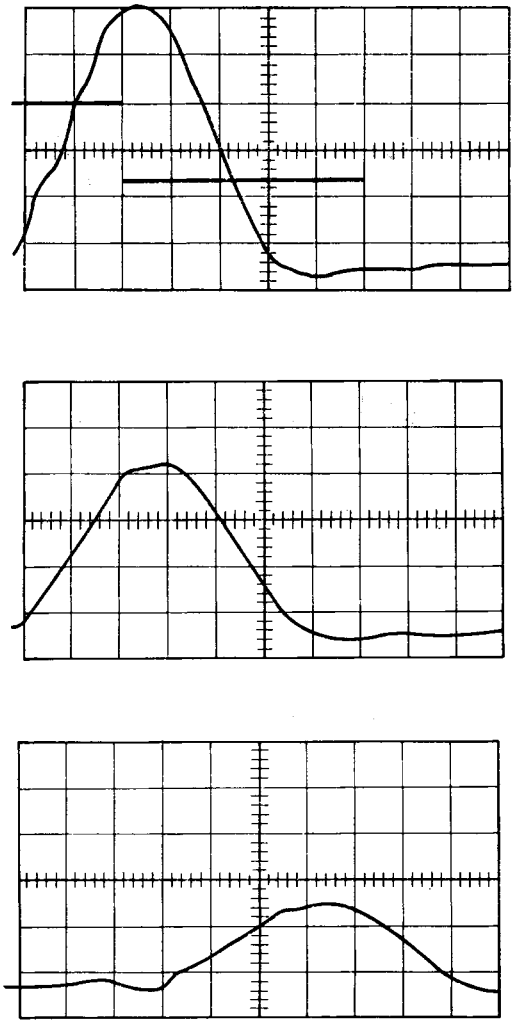

Figure 10.

In Figure 12 are two sets of oscillograms showing bending vibrations. The upper set shows the vibrations in the horizontal plane for two successive impacts. Reproducibility is good, although not as perfect as in the axial strain oscillograms. The lower set of curves compares the vibrations in the horizontal plane with those in a vertical plane. The latter are obviously of higher frequency and less damping. Presumably the frequency difference is due to a difference in the moment of inertia of the crossarm about the two axes.

The consequences of these bending strains are not easy to evaluate. For impacts of very low energy, where the strains are all within the elastic limit, they probably do not affect the results. For impacts of very large energy, such as occur when the machine is used in the way in which it was intended, the effect may not be too great.

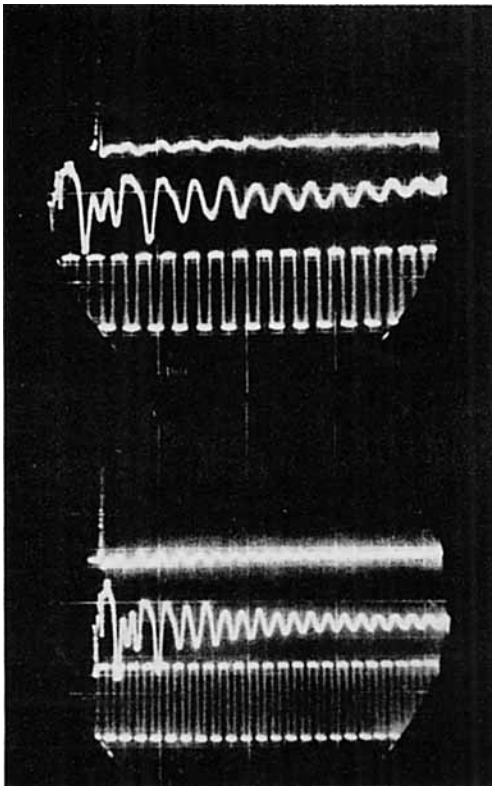

Figure 11.

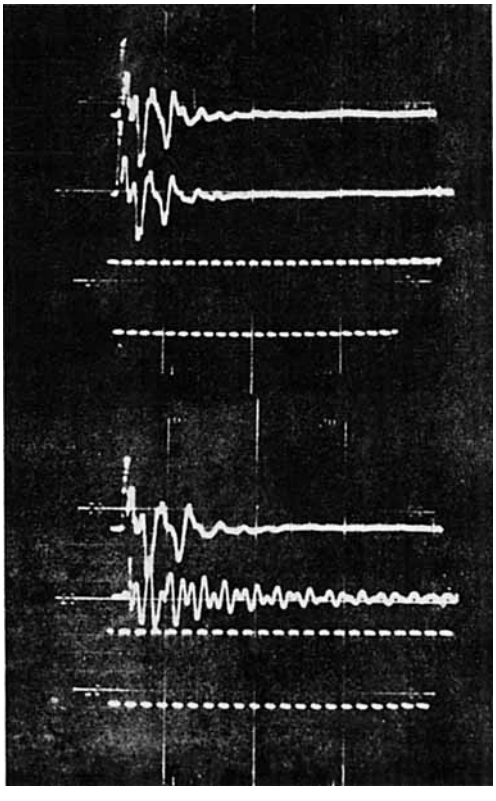

Figure 12.

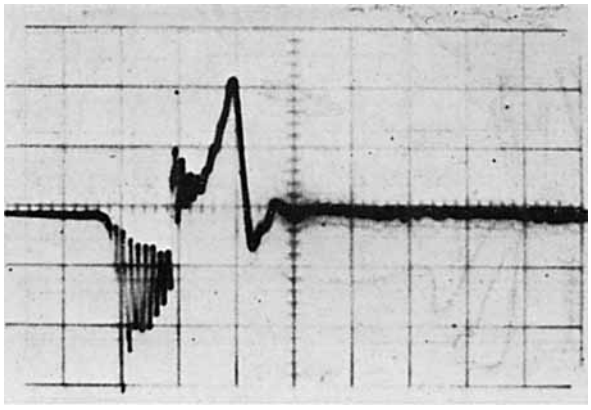

Figure 13.

But for the energy range of real interest, namely, that which is just enough to break the specimen, the bending strains so complicate the analysis that it is extremely difficult, if not impossible, to interpret the data.

This situation is not an uncommon one. The next two figures demonstrate the behavior of a different machine. Figure 13 shows the actual pulse shape for a machine whose specification was: rectangular pulse, rise time not over 1 msec., duration at least 10 msec., variations from a flat top pulse, including overshoot, ringing, and droop, not more than $\pm 5\%$. It is probable that the manufacturers of this machine was completely honest, and that at first they really thought that it was meeting the specification. However, they were using low-frequency instruments in its evaluation. It may be that they observed ringing and assumed it was the accelerometer resonance. They may have used a low-pass filter to suppress the supposed accelerometer ringing, although they would never acknowledge that they did. In any event, after many months of argument they

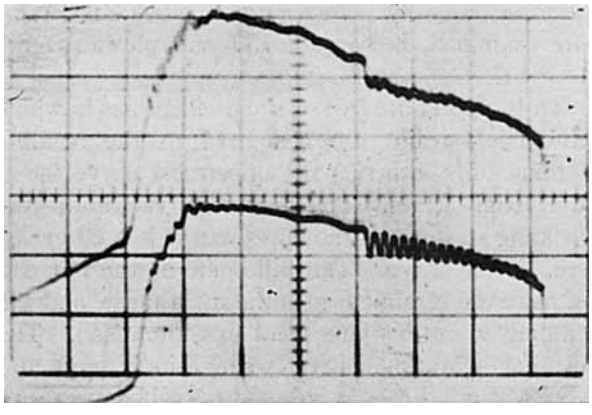

Figure 14.

agreed to remeasure one of the machines with a high-frequency accelerometer. Thereafter they were fairly conscientious in correcting the machine's defects. Figure 14 shows the pulse shape at the next-to-the-last improvement. In the final step they were able to provide a pulse with a rise time of 1.2 msec., a duration of 9 msec., a ringing of not over 10%, and a droop of about 15%. Although this did not meet the specification, it was accepted as being probably the best they could do.

It may be that some of the newer machines that have come on the market in recent years do not have the kind of defects that have been described, but the older machines that have become well established are, on the basis of what others have told us, for the most part of the same kind. As a result of the defects described, some, if not all, of the items that we test are subjected to a more severe environment than we realize. This has been discussed at length in a previous paper.[1] Suffice it to say here that the minor irregularities shown in Figure 14 could produce a strain tenfold or more greater than that produced by the main pulse if they excite a structural resonance in the part being tested.

In summary, if you plan to conduct dynamic mechanical tests with machines of the type discussed, it is wise to instrument the machine fully, using the widest possible bandwidth for the instrumentation. The electrical noise should be eliminated at the source. If the remaining irregularities are not tolerable, they too must be eliminated at the source. Nothing at all is accomplished by eliminating them only from the record by means of a filter.

PART II. A VIBRATION-FREE TEN-FOOT DROP-TESTER*

The remaining part of this report deals with work that resulted from an attempt to come directly to grips with the "fragility rating" problem. Early in the Penn State program it was decided that it would be desirable to supplement our basic research work with some "practical" tests of end items. A working hypotheses was established based on some work published by Frankland.[2] It was based on a "go-no-go" situation illustrated by the graphs in Figure 15. The argument was that there existed some velocity change, represented in Figure 15*A* by the vertical portion of the curve, for which the energy involved was too small to break

* By Howard A. Scheetz and J. Norton Brennan.

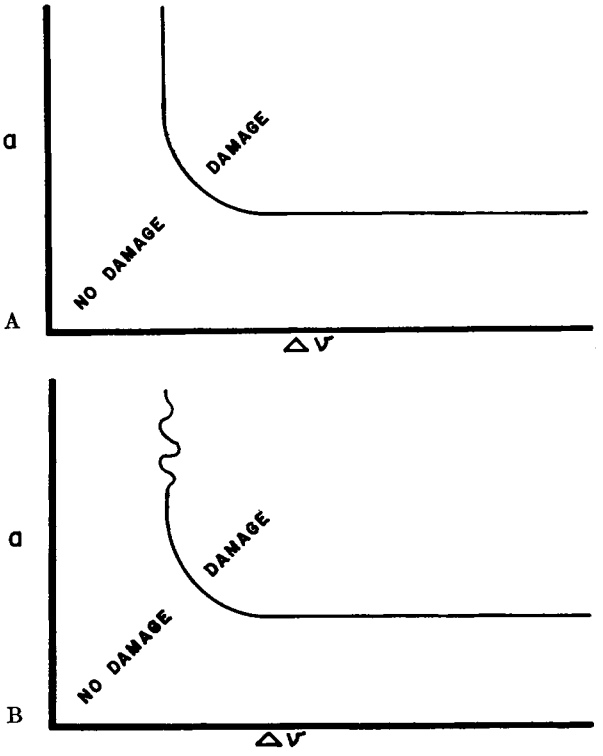

Fig. 15. Acceleration amplitude vs. total velocity change as damage criteria.

any part of the test item, and that there existed an acceleration, represented by the horizontal portion of the curve, for which the resulting strains, no matter how long the duration, could never produce failure. It was recogn zed that rise time and duration would produce squiggles in the vertical portion of the pulse, as shown in Figure 15*B*, but that their effect would probably be minor, and could be investigated later.

Existing test facilities consisted of several ballistic pendulums having drop heights up to 6 ft., a Riehle machine, already described, and a hydraulic impactor capable of producing an impulse of 100*g* over a 10-msec. period. Because of the modest capabilities of our test equipment it was found desirable to select for the initial test items things known to be fragile. As the first test item we selected a panel millivoltmeter, and established as a criterion of damage, loss of calibration. We were surprised to learn that when subjected to a 1/4-msec. impulse as large as 600*g* the meter being tested could withstand repeated impacts without limit. When the amplitude was increased to 700*g* the case cracked, but the calibration was unaffected. At still larger amplitudes, up to 2000*g*, all we could do was crack the case—no loss in calibra-

tion. This suggested that there was a need for a machine having somewhat more energy and a longer duration pulse, such as the one that is about to be described.

A. Drop-Tower Assembly

A drop tester, shown in Figure 16, consists of three main parts: an impactor upon which the test item is mounted, an anvil (pneumatic decelerator) upon which the impactor strikes, and a guidance system which maintains orientation of the impactor during its fall and controls rebound to prevent multiple impacts. The way in which the latter function is accomplished is as follows. The impactor is supported by, but is not attached to the carriage. When the impactor strikes the anvil,

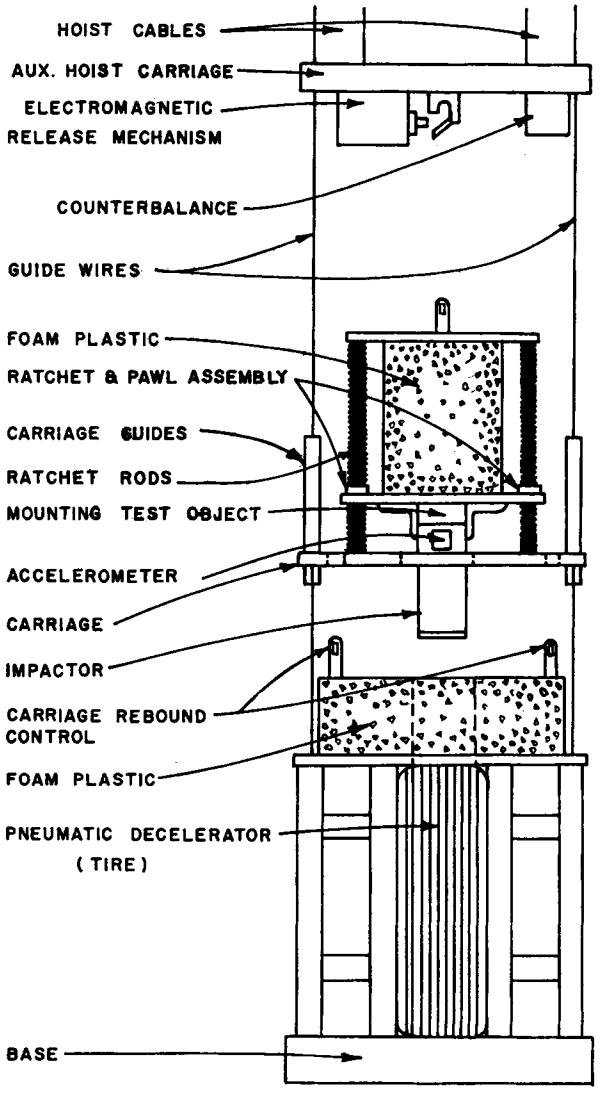

Fig. 16. Drop tower assembly.

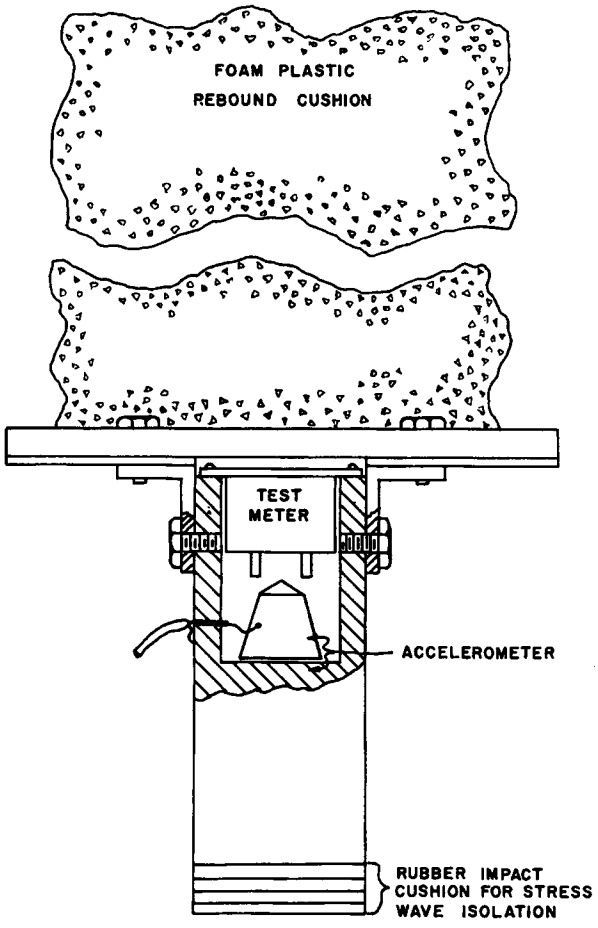

Fig. 17. Impactor-accelerometer assembly.

the carriage breaks free and travels about an inch before it strikes a polyurethan foam cushion. It is brought to rest independently of the impactor and prevented from rebounding by two toggles. Meanwhile, the impactor rebounds against a 12-in. thickness of foam plastic. When it comes to rest, it is prevented from having a second impact by a rachet pawl system. This arrangement prevents the mechanical ringing of the carriage from being transmitted to the test item, and a remarkably clean mechanical pulse results, as is shown below.

Figure 17 shows details of the impactor. It was made from a 3-in.-diameter cylindrical steel bar, with one end bored out to provide space for an integral accelerometer and the test item. An early difficulty with the impactor was that its fundamental longitudinal mode of vibration was being strongly excited. This vibration was suppressed by mounting several layers of Isomode pad on the impactor's striking surface. Various kinds of anvils were tried. Best initial results were obtained with layers of rubber pads. However,

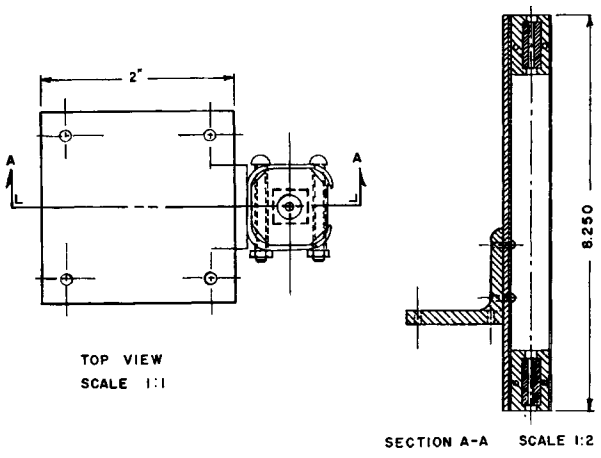

Fig. 18. Carriage guide assembly.

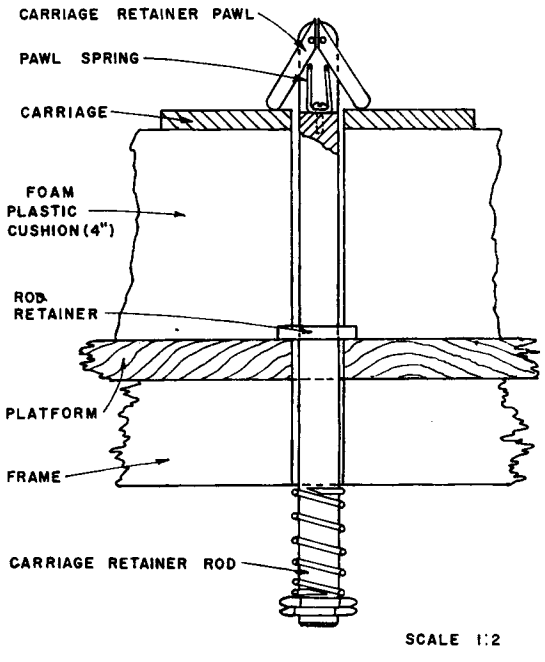

Fig. 19. Carriage retainer.

these had the disadvantage that the thickness had to be changed every time the drop height was changed. Finally, an automobile tire was tried with good success. It was simply supported on a steel and concrete foundation and restrained from horizontal motion by a wooden framework. Airplane control cable was used to guide the falling carriage by means of the guide assembly shown in Figure 18; Figure 19 shows details of the means used to prevent carriage rebound.

B. Acceleration-Measuring System

The accelerometer–impactor assembly shown in Figure 17 was originally calibrated as part of a ballistic pendulum facility as described by Nisbet.[3] This method gave an acceleration sensitivity S_1 of 120 mv./g. for the basic acceleration transducer which was also valid for use at the drop tower. Since the accelerometer traveled up and down with the impactor, a long coaxial cable was required. The increased shunt capacitance of the cable decreased the sensitivity S_2 to 103 mv./g. This was due to the fact that the piezoelectric disk acts as a charge generator which must charge up both the electrostatic shunt capacitance C_A of the disk and the external shunt circuit capacitance C_S. The resultant voltage sensitivity is therefore proportional to the total capacity, where

$$Q = CE$$

$$(Q)_{a=\text{const.}} = (C_A + C_S)E = \text{constant}$$

where a is acceleration, Q is the charge, and E denotes voltage, and

$$S_2 = S_1[C_A/(C_A + C_S)]$$

This assumes that the internal impedance of the bonded piezoelectric disk is small in comparison to the external load resistance and that the time constant formed by this impedance in series with

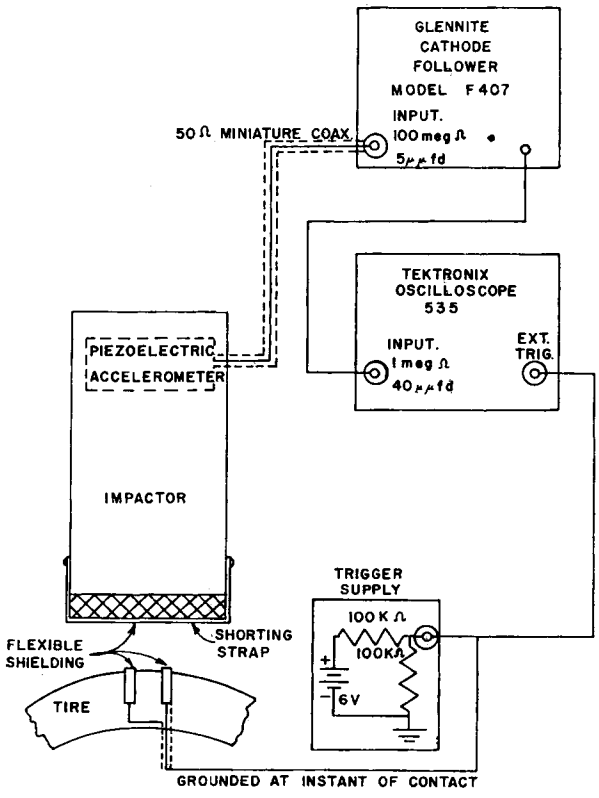

Fig. 20. Accelerometer system.

the external capacitance is small compared with the period of the highest shock frequency. Based on analogous ultrasonic delay line transducer theory, the latter assumption is valid until megacycle frequencies are approached. The former assumption is improved through the use of a cathode follower-type preamplifier (see Fig. 20) which also extends the low-frequency response. A Gulton type 407 preamplifier was used which had the following characteristics:

Input impedance:	100 megohms, 5 $\mu\mu$f.
Output impedance:	300 ohms
Gain:	0.98
Lower half-power frequency:	0.2 kcycles/sec.
Upper half-power frequency:	30 kcycles/sec. (10 v. input, 1000 $\mu\mu$f. load)
Peak input voltage:	60 v.

The acceleration sensitivity at the input to the oscilloscope with the preamplifier included became 101 mv./g.

The relatively high capacitance of the accelerometer and cable system ($C_A + C_S$) along with the high input resistance R of the cathode follower provided a combined low frequency f_1 half-power point of 0.44 cycles/sec., where

$$f_1 = 1/2\pi R(C_A + C_S)$$

and where

$$C_A + C_S = 3655\ \mu\mu\text{f}.$$

$$R = 100 \text{ megohms}$$

The equivalent time constant T for this circuit was 0.36 sec., which was much greater than the total duration of the acceleration pulse. Under these conditions, the "droop" of the acceleration pulse due to current flow in the accelerometer output circuit may be calculated by integration of the acceleration-time curve also described by Nisbet[3b]:

$$A_2(t) = A_1(t) + (1/RC) \int_0^t A_1(t)dt$$

Numerical summation for 0.5 msec. time intervals was used to obtain the droop correction shown in Figure 21. It can be seen that the correction has almost negligible effect upon the indicated acceleration pulse. Should droop become significant, the effect could be reduced by additional shunt capacitance with a sacrifice in voltage sensitivity.

The upper half-power frequency f_2 in an acceleration-measuring system is determined by four principal factors: (*a*) the lowest natural resonant frequency of the accelerometer unit, (*b*) the degree of damping present in the accelerometer unit, (*c*) the lowest natural resonant frequency of the impactor-accelerometer assembly which is excited under impact conditions, (*d*) the high frequency response of the preamplifier. Due to special construction of the accelerometer unit, a very high degree of mechanical damping was present. This extended the useable frequency range to within 80% of the natural resonant frequency. The gravest resonant frequency of the accelerometer unit was found to be about 75 kcycles/sec. Thus the accelerometer was basically

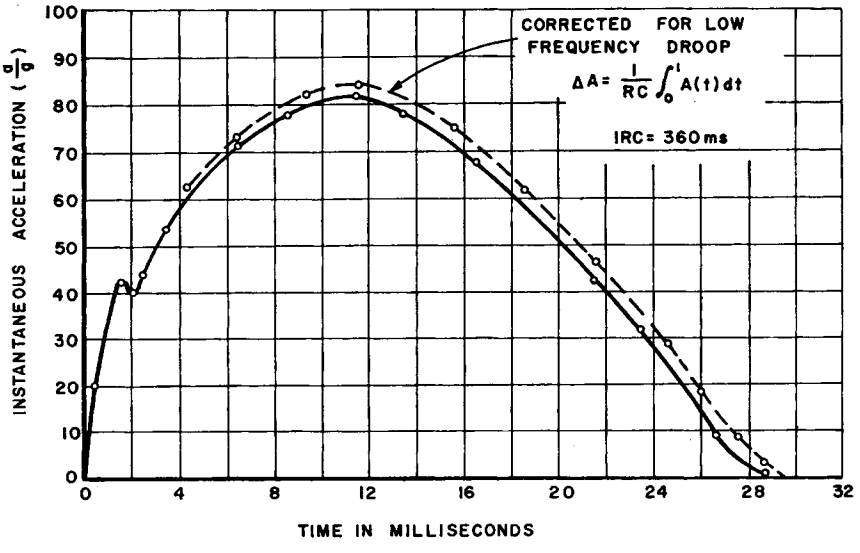

Fig. 21. Acceleration pulse characteristics with air-filled decelerator.

"flat" to 60 kcycles/sec. An electrical impulse technique was used to excite the resonant modes which were observed on the cathode-ray oscilloscope. Variation of the pulse generator load level and the pulse width permitted exciting the lowest resonant mode. Because the accelerometer assembly was soldered directly to the impactor body, the frequency dependence upon mechanical loading was fixed so that the "true" resonant frequency was determined.

The ballistic pendulum setup was used as a mechanical impulse test for determining the gravest resonant frequency of the impactor body. As noted before, this was found to be 33 kcycles/sec. The high frequency response of the cathode follower is dependent upon the input voltage level and the output load capacitance. A typical value of the upper half-power frequency would be about 30 kcycles/sec.; conservative value for the entire system would be 25 kcycles/sec. Based on the 25-kcycle/sec. bandwidth, the shortest acceleration rise time, t_r, to which the system would respond faithfully was 14 μsec., where:

$$t_r = 0.35/BW = 0.35/(f_2 - f_1)$$

where BW is a 3-db. bandwidth and f_2 and f_1 denote upper and lower half-power frequencies, respectively. The system bandwidth was more than adequate for the shock frequencies encountered to date.

A single-sweep cathode-ray oscilloscope was used for all acceleration measurements to facilitate photographing of the transient (impact) acceleration. To observe the entire leading edge of the acceleration pulse, an external trigger circuit was provided as shown in Figure 20. The trigger was initiated at the instant of contact between the flexible conductors mounted across the face of the impactor and the decelerator. Because of the time delay required for the stress pulse to propagate from the point of impact to the accelerometer mounting, the sweep began a fraction of a millisecond before the acceleration pulse, thus presenting the entire pulse.

C. Displacement-Measuring System

During the early developmental stages of the carriage assemblies, it was difficult to ascertain the lateral stability of the carriage guide system, the degree of superficial carriage vibration, etc., during the period of free fall. A displacement gage was constructed to monitor the carriage motion by using the steel guide wires in a slide-wire potentiometer circuit. Because the guide wires were composed of stainless steel with sufficient resistivity (0.22 ohms/ft.) to form a potentiometer, the displacement transducer did not require extensive design. The wire ends were insulated with strain insulators, while the portion over the guide pulleys was enclosed in insulating tubing. One wire was then used as the potentiometer, while the other merely coupled the displacement voltage to the oscilloscope input as shown in Figure 22. A pair of beryllium-copper leaf springs were mounted at the top of the carriage guide bearing to apply a counterbalanced contact pressure on the steel wire. These four contacts were electrically common, as shown in Figure 23.

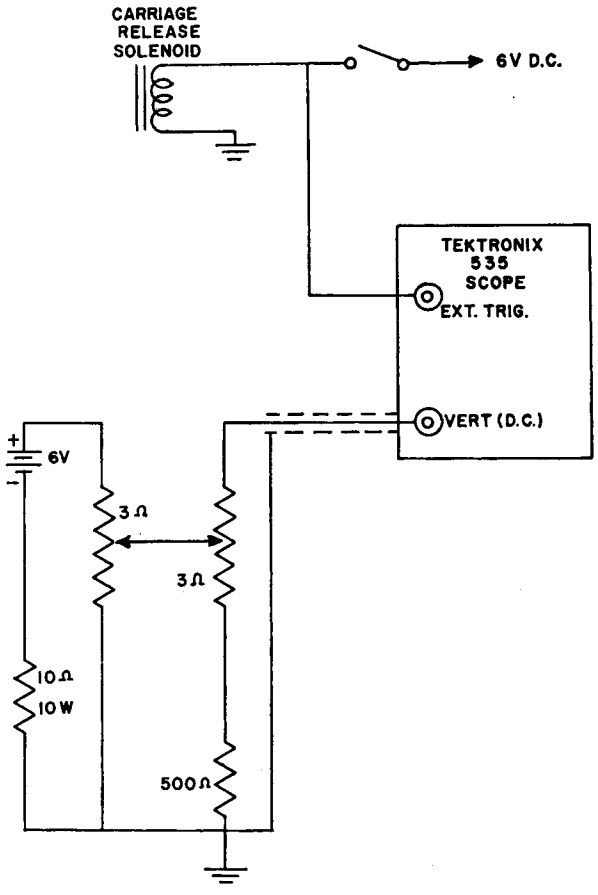

Fig. 22. Displacement gage circuit.

The output from the displacement gage was fed into a slow-sweep cathode-ray oscilloscope, and the trace was photographed after calibration of the vertical voltage sensitivity and the horizontal sweep rate. The resulting displacement–time signal (Fig. 24), was a smooth curve throughout the period of free fall, indicating that no er-

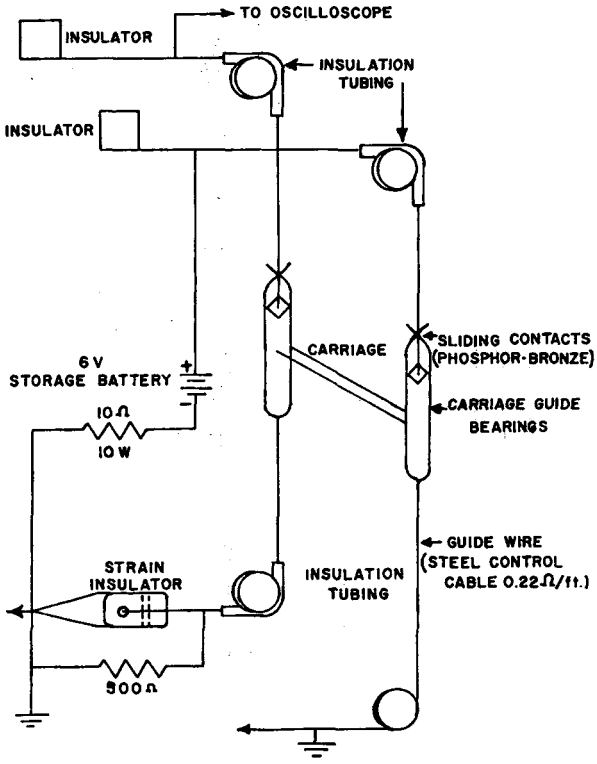

Fig. 23. Carriage displacement gage.

ratic motion of the carriage existed. Likewise the sliding contacts on the stranded steel wire performed well without introducing a high noise level.

The second and most important function of the displacement gage was to provide information on the striking or final velocity of the impactor. The slope of the displacement curve immediately before the impact was proportional to the final velocity:

$$(dx/dt)_{x=0} = V_f$$

While visual determination of this slope may be improved by expanding the oscilloscope sweep during this period, a more accurate method lies through the use of a finite difference approximation. The slope of a curve at point 0 may be approximated by a function of the ordinates of the two adjacent points to one side (points 1 and 9, respectively) as follows:

$$(dy/dt)_0 = (-3y_0 + 4y_1 - y_4)/2a$$

where: y_0, y_1, y_9 are the respective ordinates, and a is the spacing of the points along the abscissa.

Since $y_0 = 0$ for this application, the equation for the final velocity becomes:

$$v_f = (4y_1 - y_9)/2a$$

For example, for a drop height h of 120 in., $a = 100$ msec. and $y_1 = 24$ in. and $y_9 = 43$ in. (from displacement–time oscillograph)

$$V_f = \frac{4 \times 24 - 43}{2 \times 0.100} = 265 \text{ in./sec.} = 22 \text{ ft./sec.}$$

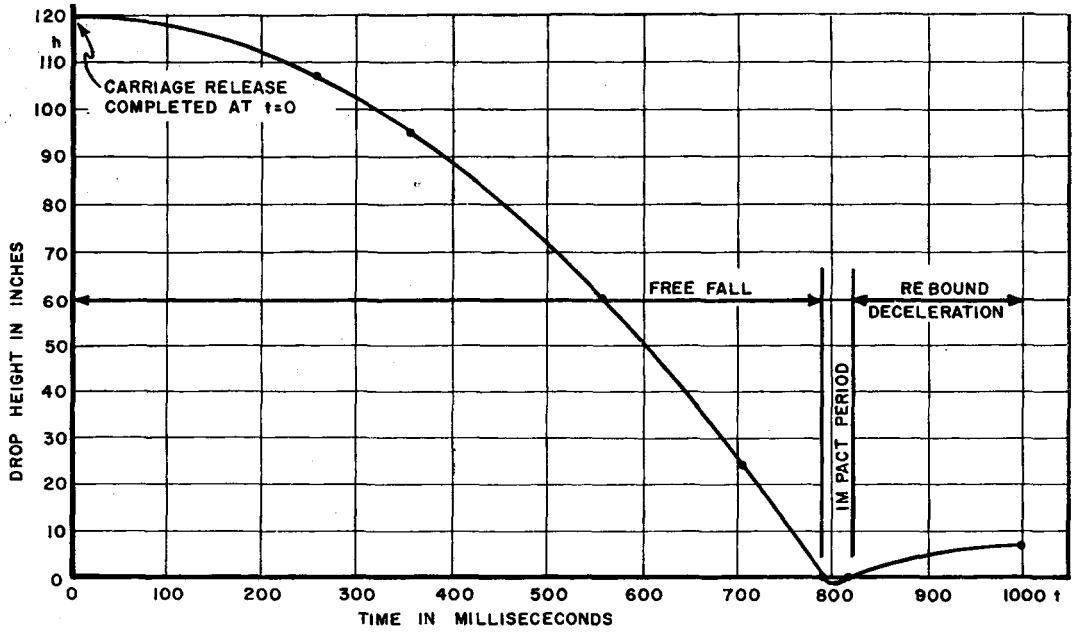

Fig. 24. Impactor displacement–time function.

An estimated accuracy for this method is within about ±5%. While many minor factors contribute to the inaccuracy, the largest and most important factor is the determination of the ordinate values at the regularly spaced points 0, 1, and 9.

The calculated striking velocity of 22 ft./sec. for the 10-ft. drop height is seen to be significantly lower than the free fall velocity *in vacuo* of 25.6 ft./sec. The true striking velocity may be used to calibrate the accelerometer, as will be shown subsequently. It is assumed that the difference is primarily due to air friction rather than carriage-guide wire friction. The drop heights were measured by a steel tape suspended from the auxiliary hoist carriage. Actual data represent the distance between the impactor striking end and the contact point on the decelerator.

D. Pneumatic Decelerator Pulse Characteristics

The acceleration–time pulse produced with the pneumatic decelerator was a nearly smooth curve of the skewed half-sinusoid type curve as shown in Figure 21 for the 10-ft. drop height. Although the pulse length increased slightly with drop height, the pulse shape remained relatively constant. The peak acceleration reached for each drop height is shown in Figure 25. For low drop heights, the peak g level was higher than would be expected from a linear, spring-mass, viscous-damped system as shown by the curve. This seems reasonable if one considers that for small deflection the tire would behave as a hollow toroid with a concentrated, external load acting normal to the surface. The equivalent spring constant would be primarily due to the rigidity of the cylinder walls. For large deflections the wall curvature would be reversed due to buckling at the impact point which makes the spring constant dependent primarily upon the internal air pressure. The latter case would have a smaller spring constant and therefore less relative peak acceleration.

The striking velocity may be obtained from the acceleration–time data by numerical integration, providing appropriate corrections are included. In general, the equation of velocity change is:

$$v_1 - v_2 = \int_{t_1}^{t_2} A(t)dt$$

During the period of free fall prior to the impact, air friction acts on the moving mass to decrease the velocity and extend the drop time. This decreases the average acceleration below the $1g$ force of gravity, leaving an equation with three unknowns:

$$-V_f = \int_0^t A(t)dt$$

It is noteworthy that piezoelectric accelerometers will not indicate static accelerations as are encountered in the gravitational field.

A better approach to velocity determination would be to consider the time interval $\Delta_1 t$ from the instant of impact to the time corresponding to the peak acceleration. For a system with no viscous damping, the velocity will be zero at the instant of the peak acceleration. From the acceleration pulse correction for low frequency "droop" as

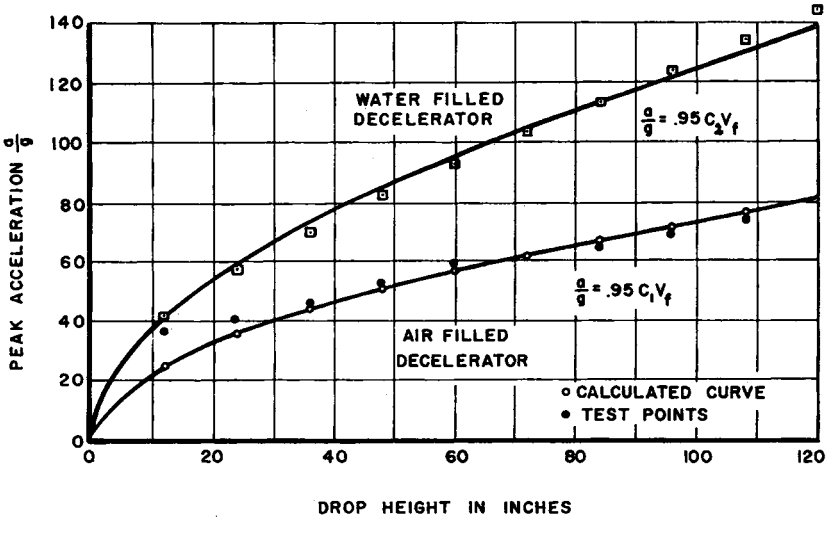

Fig. 25. Peak acceleration vs. drop height.

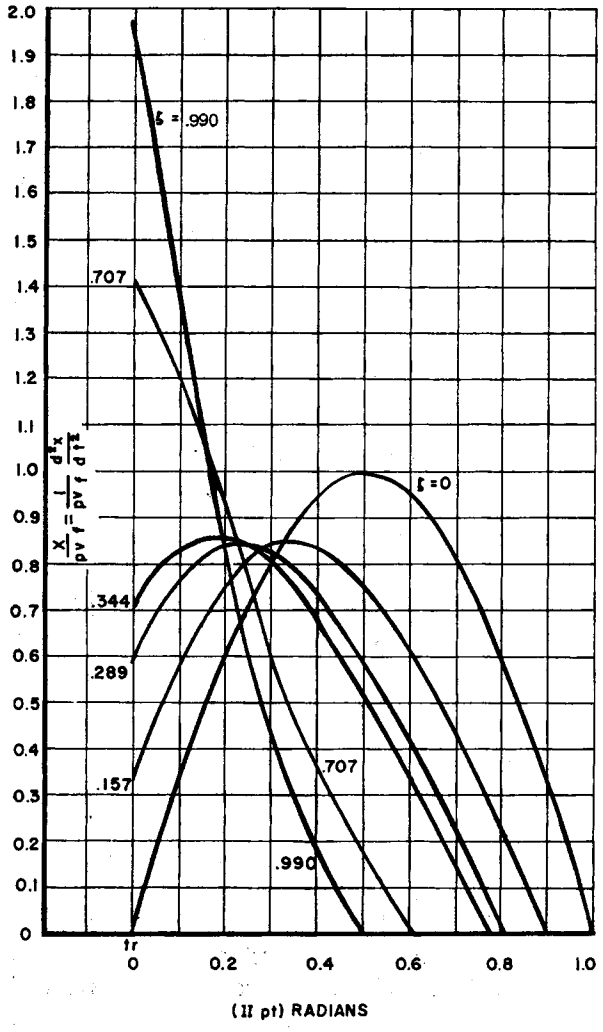

Fig. 26. Acceleration vs. damping factor for a solid damped (hysteresis) system.

shown in Figure 21, the striking velocity was calculated to be

$$V_f = \sum_{t=0}^{11.5\times10^{-3}} A(t)\Delta_2 t = 23.3 \text{ ft./sec.}$$

where $\Delta_2 t$ was a time increment of 0.5 msec.

The principal error in this procedure lies in the determination of the peak acceleration point A_{pk}. To minimize this error and that of numerical integration of the area, the oscilloscope photographs were enlarged on a microcard reader and traced onto larger paper (24 magnification). For a time uncertainty of 11.5 ± 0.3 msec., the velocity uncertainty ΔV becomes $\pm 3.5\%$, where

$$\Delta V = \Delta_1 t A_{pk}/\Sigma A(t)\Delta_2 t$$

It is interesting to note that the low-frequency correction amounted to only 1.4% of the indicated velocity. A less obvious error exists when the system has damping, for here the velocity lags the acceleration by more than the 90° usually associated with simple harmonic motion. The true phase angle is dependent upon the damping factor ζ. For a large damping factor, the zero velocity point would occur after the point of peak acceleration had occurred. Since this function contains both sine and cosine terms, the acceleration to displacement phase shift noted for the viscous damped case also appears for the solid damped case. Solving for the value at $t = 0$ (or more precisely, for $t_1 = t_r$), the initial acceleration becomes:

$$(d^2x/dt^2)_{t=0} = -2\zeta p V_f$$

where p is the natural frequency in rad./sec.

This is the same value as obtained for the viscous damped case. Thus, it would appear that the mere presence of a damping term in the exponential form that causes the initial jump in acceleration rather than the type of damping that is being considered. The discontinuity of the acceleration pulse illustrated in Figure 21 may be expected for any highly damped system under impact conditions. Figure 26 presents a more complete picture for the solid damped case. As the damping factor increases and approaches critical damping, the duration of the acceleration function becomes increasingly shorter, since the period remains constant while the phase shift is increasing. Thus, even higher frequency components will be present in the shock spectrum of the solid damped case.

E. Hydraulic Decelerator

In order to increase the peak acceleration available without increasing the height above the ceiling level, an investigation of the fixed variables in the deceleration system was begun. A series of tests were made at a drop height of 10 ft. For a constant striking velocity, increasing the peak acceleration level requires a decrease in the duration of the acceleration pulse. One way of accomplishing this is to increase the effective spring constant of the decelerator. This was done by filling the inner tube with water. Several tests were made with increasing water levels, each of which increased the peak g level. To minimize the effect of the residual trapped air, the final filling was done by evacuating the inner tube with a mechanical roughing pump before filling with water. During the last stages, water was pumped

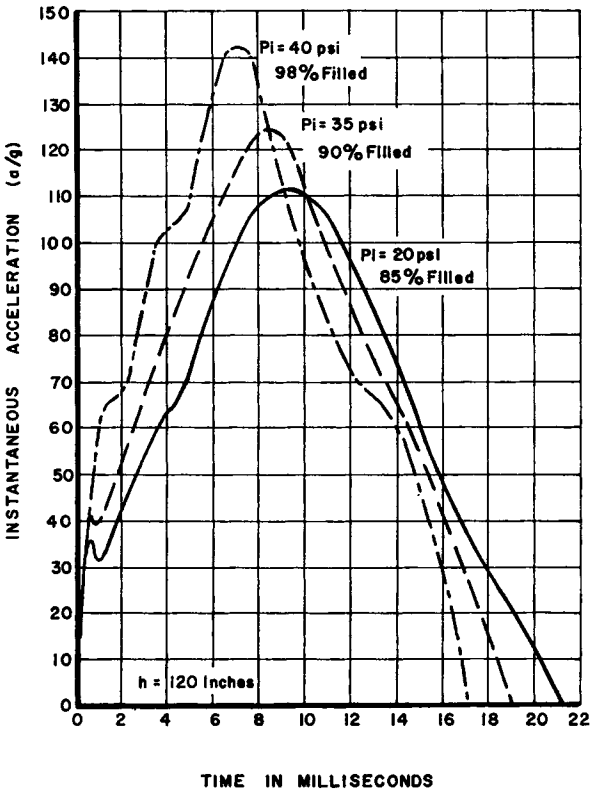

Fig. 27. Acceleration pulse characteristics with the hydraulic decelerator.

in to reach a pressure within the tube of 40 psi. A small air pocket did exist, but the tire deformation with a 10-ft. drop height was sufficient to insure contact with the water level. The equivalent spring constant was increased significantly, resulting in a doubling of the peak g level.

Figure 27 illustrates the shape of the acceleration pulse obtained with the hydraulic decelerator. It can be seen that both the volume and pressure of the entrapped air affect the pulse shape. For the case of the highest degree of filling with (about 98% water), the effective damping factor was higher, as shown by the a_1/a_{max} ratio. A measure of the actual damping present for this case was obtained from rebound height measurements with the ratchet mechanism removed. The natural logarithm of the ratio of drop height h_1 to rebound height h_2 then gives the logarithmic decrement δ for one-half cycle of the vibrational system:

$$\delta = (1/n) \ln (h_1/h_2)$$

The damping factor ζ for a viscous damped system may be calculated from:

$$\zeta = \delta/\sqrt{(2\pi)^2 + \delta^2}$$

For the 10-ft. drop height, the following data were obtained: drop height = 120 in.; rebound ratio, $h_1/h_2 = 2.7$; logarithmic decrement $\delta = 2.0$; damping factor $\zeta = 0.3$.

F. Shock Testing of a Panel Meter Movement

After completion of the initial tests with the pneumatic decelerator, a series of tests was made with a panel-type milliammeter mounted in the impactor. The meter selected was a Westinghouse type RX-33 milliammeter with a d.c. rating of 50–0–100 ma. which was available in quantity at moderate cost on the surplus market. The plastic case had a $2^1/_4$-in. square face with a $2^1/_{16}$-in. diameter body $1^5/_{16}$ deep. The case body fit inside the impactor with the mounting surface resting against the end of the impactor. The tapped mounting screw holes were drilled through to permit fastening (four screws) to the impactor. The shock received by the meter was in the form of a deceleration pulse applied normal to the meter face. The deceleration force (meter weight = 148 g.) was applied to the meter through the panel mounting surface so that the mounting screws were not required to transmit or withstand these forces.

Before each shock test, the meter movement was calibrated at seven different current levels. Afterwards, the meter was recalibrated at the same points to determine if any change had occurred. With the pneumatic decelerator, the deceleration pulse (or acceleration pulse if considered with respect to the impactor body) was the same as shown in Figure 21. Under these conditions (10 ft. drop), no physical damage occurred nor was the meter calibration affected.

The hydraulic decelerator previously described was used for additional meter tests. Again, no damage occurred. Another test was made with a 6-in. diameter plywood disk resting on the decelerator to increase the contact area. This effectively increased the spring constant and the peak acceleration. The acceleration pulse was now trapezoidal-shaped with a peak of $173g$ and a duration of 13 msec. (zero amplitude level). Meter tests with the latter shock characteristics produced no damage and did not affect the meter calibration. A summary of the meter tests is shown in Figure 28.

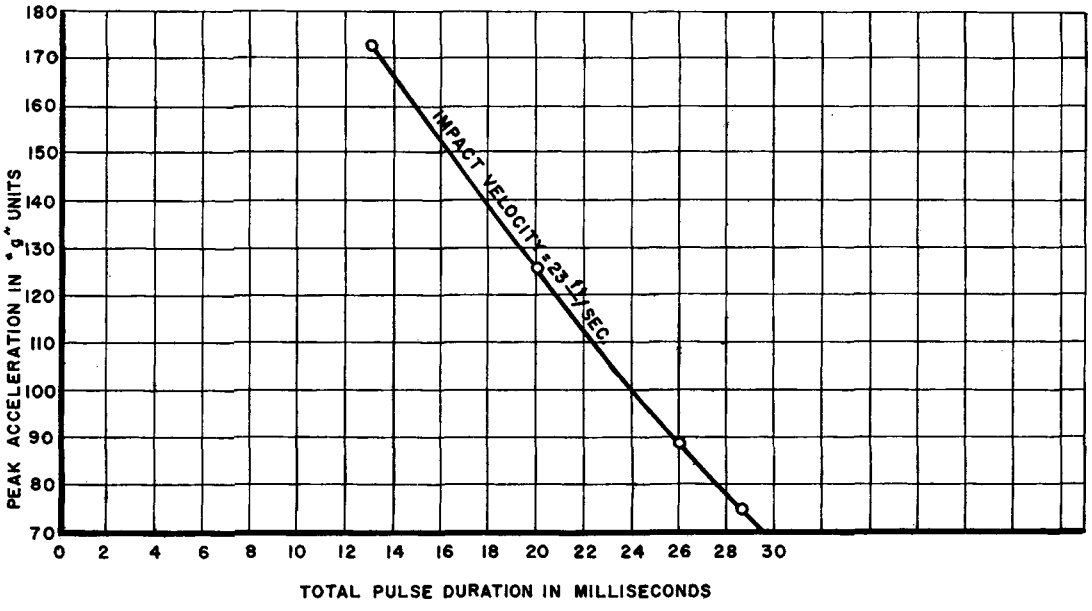

Fig. 28. Panel meter shock test data, meter face normal to the impact direction.

G. Evaluation of Cushioning Material

The analysis of highly damped deceleration systems indicated an initially high acceleration "step" for two different types of damping. Paper honeycomb is frequently used as a cushioning material. Since it absorbs impact energy during collapse of the paper structure, it is effectively a damped system and should produce the same sort of initial acceleration step. Two series of tests were made with 3-in. thick disks of paper honeycomb to determine the validity of this prediction. The first series consisted of a 5-in. diameter disk resting on the hydraulic decelerator with the 3-in. diameter impactor body penetrating the disk from the 10-ft. drop height. A rapidly rising acceleration step was present in the resulting acceleration pulse. The paper disk was, however, sheared by the impactor so that only the central portion collapsed in a typical manner. To circumvent this problem, 3-in. diameter disks were tied to the impactor and dropped with it providing complete collapse of the honeycomb. The resulting characteristics are shown in Figure 29. The initial acceleration step

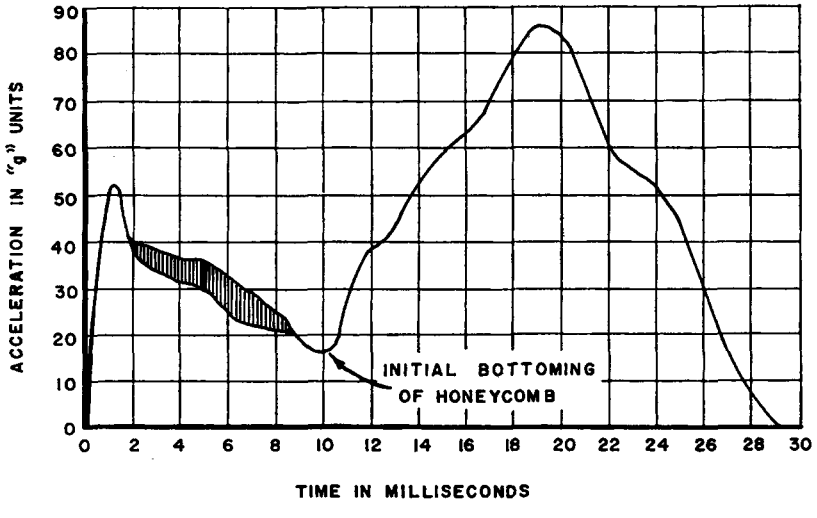

Fig. 29. Acceleration pulse characteristics with the hydraulic decelerator and paper honeycomb cushioning.

was present followed by a decrease in acceleration level as the honeycomb collapsed. As complete collapse or "bottoming" was attained, the remaining impact energy deflected the hydraulic decelerator, producing a second peak similar to the pulse shown in Figure 27. The paper honeycomb was purposely overloaded to clearly demonstrate one specific point: that significantly high peak accelerations may be reached before any significant impact energy has been absorbed by the honeycomb structure collapse. Furthermore, the rise rate of the initial acceleration which is primarily determined by the acoustic properties of the base material contains high frequencies which may not be reproduced with low-frequency accelerometer systems. These same high frequencies could excite resonances within a loaded platform not expected from the half-sinusoidal pulse-shape approximation sometimes encountered.

The paper honeycomb used was not a standard grade, but rather a sample expanded to provide a cell size about $^{7}/_{16}$ in. width across flats. This was used merely to indicate the presence of the initial acceleration step and not to provide specific force-time data for a particular grade. The initial modulus of elasticity was estimated from typical dynamic stress–strain curves[4] to be approximately 3000 psi. This is several times higher than the value for rubber (E = 300 psi) indicating a higher rise rate of acceleration would be present. In Figure 29, the rise time is seen to be under 1 msec.

Conclusion

The drop tester that has been described provides a vibration-free means for impact testing of small test items and cushioning materials at velocities up to 23 ft./sec. Impulses ranging up to 85g at 29 msec. and up to 173g at 13 msec. may be produced.

Acknowledgement is due the U. S. Naval Nuclear Ordnance Evaluation Unit, Kirtland Air Force Base, Albuquerque, New Mexico, and to the Continental Can Company, Central Research and Engineering Division, Chicago, Illinois, who supported the preparation of this paper.

References

1. Nisbet, J. S., and J. N. Brennan, *J. Acoust. Soc. Am.*, **29**, 837 (1957).

2. Frankland, J. M., *Proc. Soc. Exptl. Stress Anal.* **6**, No. 2, 7 (1948).

3. (a) Nisbet, J. S., "A study of accelerometer calibration systems," M. S. thesis, Pennsylvania State University, August 1957, p. 30; (b) *idem., ibid.*, p. 18.

4. Turnbow, J. W., H. Matlock, and J. N. Thompson, "Characteristics of paper honeycomb under dynamic loading," Quartermaster Contract DA 19-129-QM-150, Project No. 7-87-03-004B, University of Texas, August 31, 1956.

Synopsis

It has been shown that use of wide-band instrumentation in dynamic mechanical measurements can reveal the presence of high-frequency ringing and other mechanical defects in the wave form. The use of low-pass filters to suppress electrical noise can hide such defects. It is therefore better to eliminate the electrical noise at the source. If the mechanical irregularities in the waveform are not tolerable, they must be removed by improving the design of the testing device. The drop tester described in this report illustrates one possible way in which this may be done.

Résumé

On montre que l'emploi d'instruments à large bande pour les mesures mécaniques dynamiques peut révéler la présence de sifflements de haute-fréquence et d'autres défauts mécaniques sous la forme d'onde. L'emploi de filtres passe-bas pour supprimer le bruit de fond électrique peut masquer de tels défauts. Il est cependant préférable d'éliminer le bruit de fond électrique à la source. Si les irrégularités mécaniques sous la forme d'onde ne sont pas tolérées, elles peuvent être écartées en perfectionnant l'appareillage. L'appareillage décrit dans ce rapport illustre une voie possible pour arriver à ce but.

Zusammenfassung

Es wurde gezeigt, dass die Verwendung von Weitbandinstrumenten bei dynamisch-mechanischen Messungen das Vorhandensein von Hochfrequenzund anderen mechanischen Defekten in der Wellenform aufdecken kann. Die Verwendung von Filtern niedriger Durchlässigkeit zur Unterdrückung des elektrischen Rauschens kann solche Defekte verdecken. Es ist daher besser das elektrische Rauschen am Ursprung zu beseitigen. Wenn die mechanischen Unregelmässigkeiten der Wellenform nicht zulässig sind, müssen sie durch Verbesserung der Konstruktion der Prüfvorrichtung ausgeschaltet werden. Der in der vorliegenden Mitteilung beschriebene Falltester zeigt einen möglichen Weg, auf welchem das erreicht werden kann.

Received September 26, 1960